Dyes and Pigments 94 (2012) 103–112

Contents lists available at SciVerse ScienceDirect

Dyes and Pigments

journal homepage: www.elsevier.com/locate/dyepig

Photophysical properties and photostability of novel symmetric polycyclicphenazine-type fluorescent dyes and the dye-doped films

Haruka Egawa Ooyama [a,**], Takashi Ide [a], Hiroharu Yamasaki [b], Asuka Harada [b], Yuki Nagahama [b], Ayumi Ono [b], Katsuhira Yoshida [a,b,*]

[a] Department of Applied Science, Graduate School of Integrated Arts and Science, Kochi University, Akebono-cho, Kochi 780-8520, Japan
[b] Department of Applied Science, Faculty of Science, Kochi University, Akebono-cho, Kochi 780-8520, Japan

ARTICLE INFO

Article history:
Received 31 May 2011
Received in revised form
13 November 2011
Accepted 27 November 2011
Available online 6 December 2011

Keywords:
Fluorescent dye
Photophysical property
Photostability
Fluorescent polymer film
Wavelength conversion
Polycyclicphenazine dye

ABSTRACT

Novel symmetric polycyclicphenazine-type fluorescent dyes have been synthesized and characterized in solution and in polymer films. The dyes exhibited two strong absorption bands at around 365–428 nm and 519–567 nm and an intense fluorescence band at around 560–600 nm (Φ = 0.70–0.87) in 1,4-dioxane. The dye-doped polymer films showed excellent wavelength conversion function that efficiently convert ultraviolet and yellow lights into red light (Φ = 0.61–0.92). Moreover, the photostability of the dye-doped PS, PMMA, and PLA films has been investigated.

1. Introduction

Photosynthesis and photomorphogenesis in plant growth are significantly controlled by light quality. In general various type wavelength conversion films such as UV, visible and near-infrared light absorbing films have been used for a regulation of plant growth [1–5]. It is known that red light efficiently promotes plant growth in many kinds of plants [6–8]. However, there are few reports on fluorescent dye-doped films evaluated as wavelength conversion films [9,10]. It is known that blue light also promotes the plant growth as well as red light. Therefore, we planned the creation of wavelength conversion films that can transmit the blue light and can convert the ranges of ultraviolet and yellow lights into the range of red light by using fluorescent dyes. To develop the fluorescent dyes which satisfy the conditions of the superscription, we have performed the semi-empirical molecular orbital calculations (PM 3 and INDO/S) and estimated approximately the absorption wavelengths of the dye molecules. In this study, we have designed and synthesized novel symmetric polycyclicphenazine-type fluorescent dyes (**2**, **6**, **9**). The photophysical properties of the dyes and the dye-doped polymer thin films have also been investigated. Moreover, the photostability has also been investigated to use the doped films as a substitute for plant growth regulators for PLB proliferation [11,12] (scheme1).

2. Result and discussion

2.1. Semi-empirical MO calculations (PM3, INDO/S)

We have carried out semi-empirical molecular orbital (MO) calculations for the designed fluorophores **2**, **6** and **9** to elucidate the difference of photophysical properties. The structures of these compounds were optimized by MOPAC/PM3 [13] and then the electron transition spectra were calculated by the INDO/S [14–16]. The calculated first and second absorption wavelengths and the transition character of the bands are collected in Table 1. The changes of electron density accompanying the first electronic excitation (HOMO → LUMO) are shown in Fig. 1, which reveal the migration of intramolecular charge transfer from the dibutylamino groups as donor to the central pyrazine ring as acceptor. The calculated first and second absorption wavelengths of **2**, **6** and **9**

* Corresponding author. Tel.: +81 88 844 8296; fax: +81 88 844 8359.
** Corresponding author.
E-mail address: kyoshida@kochi-u.ac.jp (K. Yoshida).

0143-7208/$ – see front matter © 2011 Elsevier Ltd. All rights reserved.
doi:10.1016/j.dyepig.2011.11.010

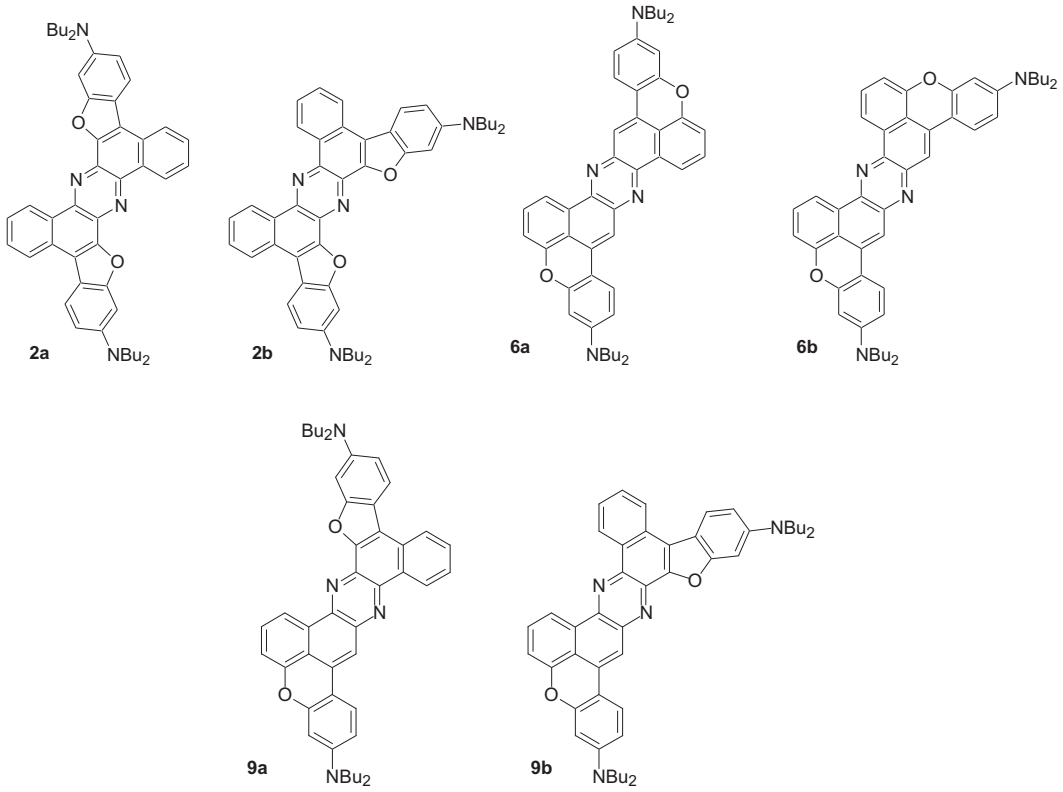

Scheme 1. Chemical structure of fluorescent dyes **2**, **6** and **9**.

Table 1
Calculated absorption spectra for the symmetric phenazine-type fluorescent dyes **2**, **6** and **9**.

Compound	μ[D][a]	Absorption (calc.)		CI component[c]	$\Delta\mu$[D][d]
		λ_{max}/nm	F[b]		
2a	0.00	438	0.88	HOMO → LUMO (85%)	0.00
		371	0.31	HOMO → LUMO+1 (54%)	
				HOMO-2 → LUMO (27%)	
2b	0.43	426	0.75	HOMO → LUMO (85%)	3.92
		347	1.17	HOMO-1 → LUMO+1 (67%)	
				HOMO → LUMO+2 (8%)	
				HOMO-3 → LUMO (5%)	
				HOMO → LUMO (4%)	
6a	0.00	440	1.14	HOMO → LUMO (87%)	0.00
		363	0.53	HOMO → LUMO+1 (63%)	
				HOMO-2 → LUMO (17%)	
				HOMO-1 → LUMO+2 (4%)	
6b	2.31	432	1.03	HOMO → LUMO (87%)	0.32
		334	1.27	HOMO-1 → LUMO+1 (59%)	
				HOMO → LUMO+2 (14%)	
				HOMO-5 → LUMO (3%)	
				HOMO-2 → LUMO (3%)	
				HOMO → LUMO (2%)	
9a	1.57	439	1.00	HOMO → LUMO (86%)	0.68
		367	0.39	HOMO → LUMO+1 (57%)	
				HOMO-2 → LUMO (20%)	
				HOMO → LUMO (4%)	
9b	1.25	430	0.88	HOMO → LUMO (86%)	2.77
		341	1.25	HOMO-1 → LUMO+1 (64%)	
				HOMO → LUMO+2 (11%)	
				HOMO-4 → LUMO (3%)	
				HOMO → LUMO (3%)	

[a] The values of the dipole moment in the ground state.
[b] Oscillator strength.
[c] The transition is shown by an arrow from one orbital to another, followed by its percentage CI (configuration interaction) component.
[d] The difference in dipole moment between the excited and the ground states.

were 428–442 nm and 334–370 nm, respectively. Moreover, the first absorption wavelengths and its oscillator strengths were increased in the order of **2b** (426 nm, $f = 0.75$) < **9b** (430 nm, $f = 0.88$) < **6b** (432 nm, $f = 1.03$), and **2a** (438 nm, $f = 0.88$) < **9a** (439 nm, $f = 1.00$) < **6a** (440 nm, $f = 1.14$), respectively. It was anticipated that the fluorophores which contain the benzopyran ring exhibited the first absorption band of higher intensity at longer wavelength region than the fluorophores which contain the benzofuran ring. It is known that the absorption wavelengths of INDO/S calculations are blue-shifted by ca. 50–120 nm than the experimental values [17,18]. Therefore, we expected that the fluorophores **2**, **6** and **9** could convert the ranges of green–yellow lights into the range of red light.

2.2. Synthesis of symmetric polycyclicphenazine-type fluorescent dyes *2*, *6* and *9*

The synthesis of symmetric phenazine-type fluorophores **2a**,**2b**, **6a**,**6b** and **9a**,**9b**, which are structural isomers, is shown in Schemes 2 and 3, respectively. We used polycyclic *o*-quinone derivatives **1** and **3** as a starting material [19]. As shown in Scheme 2, the fluorophores **2a** and **2b** were synthesized by dimerization reaction of the *o*-quinone **1** in the presence of ammonium acetate. The isomers **2a** and **2b** were obtained in 18% and 20% yields, respectively. Pyrazine skeletons were generally constructed by the condensation reaction of *o*-quinones with diamine compounds [20,21], however, this reaction can directly construct the pyrazine skeleton. Although the synthesis of the fluorophores **6** and **9** was also tried by the same reaction conditions, these reactions did not proceed smoothly. Therefore, we examined the different synthetic method as shown in Schemes 3 and 4. The *o*-quinones **1** and **3** were allowed to react with hydroxylamine to give the dioximes **4** and **7** which were

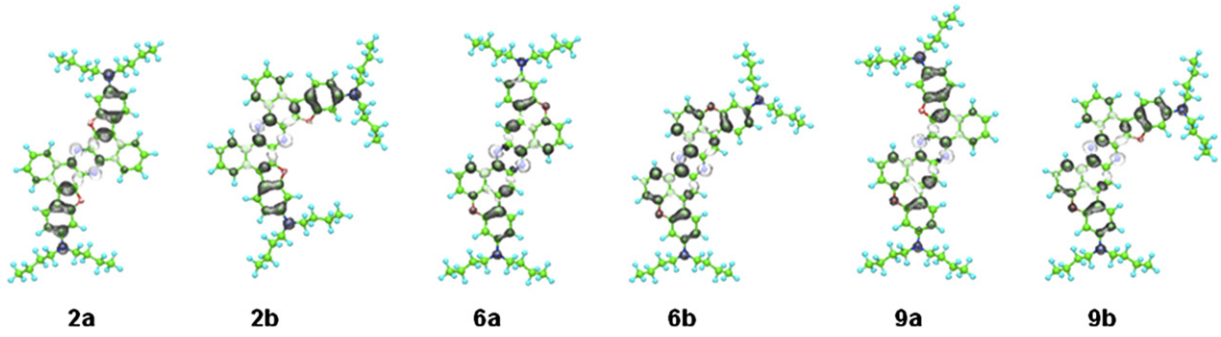

Fig. 1. Calculated changes in electron density accompanying the first electronic excitation of the symmetric phenazine-type fluorescent dyes **2**, **6** and **9**. The black and white lobes signify degreases and increase in electron density accompanying the electronic transition, respectively. Their areas indicate the magnitude of the electron density change.

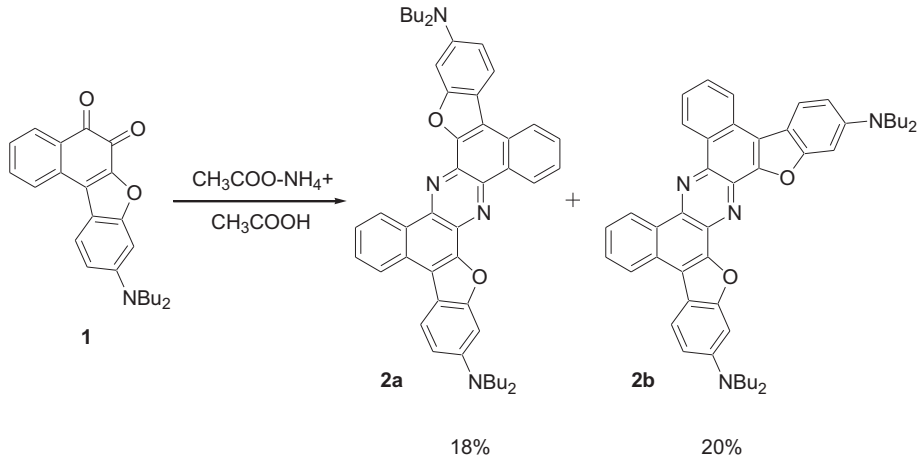

Scheme 2. Synthesis of the symmetric phenazine-type fluorescent dyes **2a** and **2b**.

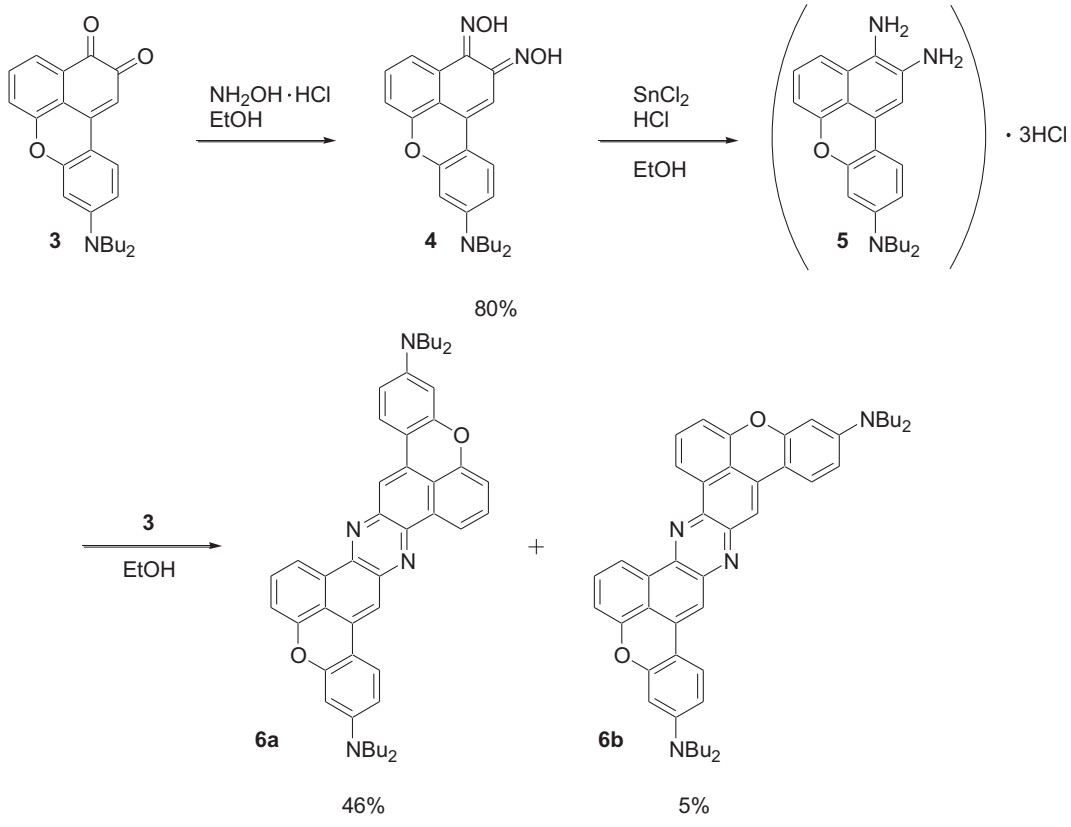

Scheme 3. Synthesis of the symmetric phenazine-type fluorescent dyes **6a** and **6b**.

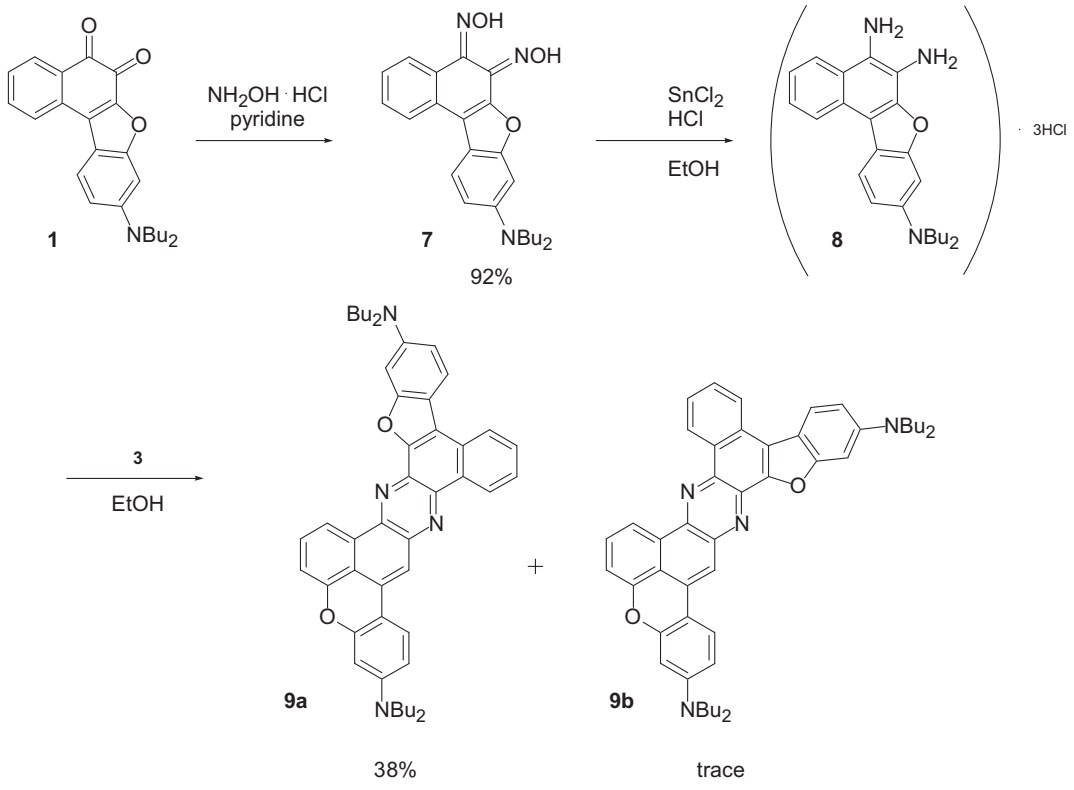

Scheme 4. Synthesis of the symmetric phenazine-type fluorescent dyes **9a** and **9b**.

then reduced with tin chloride to give the corresponding amine hydrochloride salts **5** and **8**, respectively. The salt **5** was followed to react with the quinone **3** to produce the isomers **6a** and **6b** in 46% and 5% yields, respectively. On the other hand, from the reaction of the salt **8** with the *o*-quinone **3**, the isomers **9a** and **9b** were synthesized in 38% and trace yields, respectively. These compounds were completely characterized by ^{1}H-NMR, IR, and elemental analysis. The identification of their chemical structures was carried out by comparison of the observed and calculated UV–VIS spectra for the compounds **2**, **6** and **9** and the X-ray crystal analysis of the compound **2b** described in the next section.

2.3. X-ray crystal structure of *2b*

To confirm the steric configuration of the compound **2b**, the X-ray crystal structure analysis was performed. The experimental details and the crystal data are described in the experimental section. The crystal system was a monoclinic space group $P2_1/a$ with $Z = 4$. As shown in Fig. 2, the crystal was found to be a clathrate

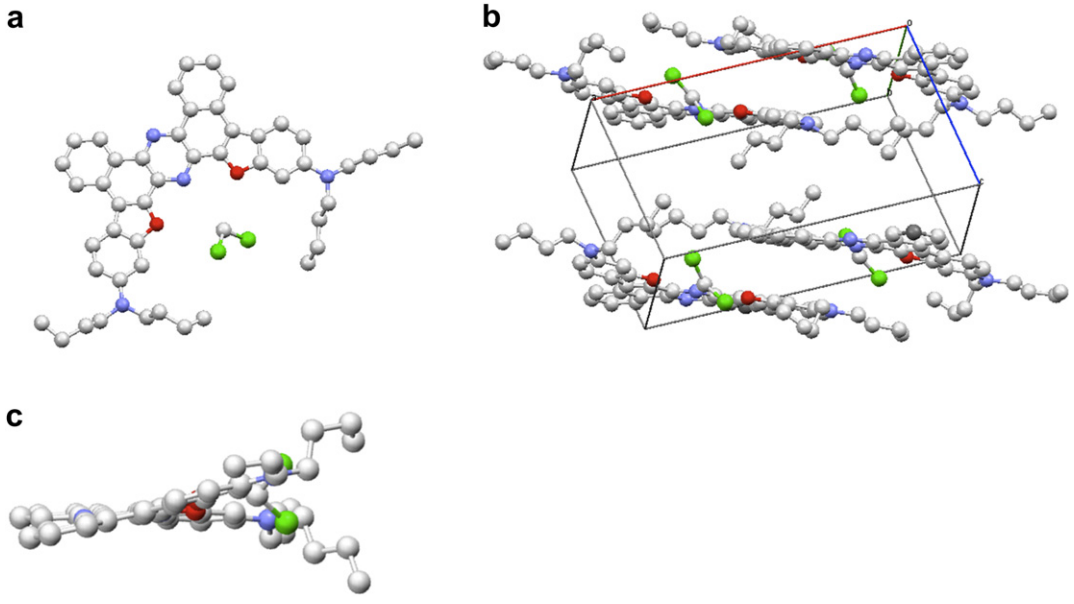

Fig. 2. Molecular structure and crystal paking of **2b**: (a) a molecular structure, (b) a stereoview of the molecular packing structure, and (c) a side view.

compound which consisted of **2b**:CH_2Cl_2 (1:1) arranging in a "bricks in a wall" fashion and the compound **2b** was confirmed to be a **b**-isomer. Moreover, the X-ray crystal structure analysis demonstrated that the molecule of **2b** was twisted at the central pyrazine part and the angle between the two π-planes of benzofuronaphthalene moieties was ca. 15.0°. For the other fluorophores, we could not get good crystals suitable for the X-ray crystal analysis.

2.4. Spectroscopic properties of symmetric polycyclicphenazine-type fluorescent dyes *2*, *6* and *9* in solution

Absorption and fluorescence spectral data are summarized in Table 2. Figs. 3 and 4 show the absorption and fluorescence spectra of the compounds **2**, **6** and **9** in 1,4-dioxane. The fluorophores **2**, **6** and **9** exhibited two major absorption bands at around 519 nm–567 nm (ε_{max} = 36,100–54,000) and 300–450 nm (ε_{max} = 35,600–62,300) and their absorption maxima were red-shifted in the order of **2b** < **9b** < **2a** < **6b** < **9a** < **6a**. From this result, it was found that the absorption wavelength of the **a**-isomer was longer than that of the corresponding **b**-isomer. Moreover, comparing among the chromophores, the absorption wavelength was red-shifted in the order of **2** < **9** < **6**. These experimental results agreed well with the results of the MO calculation. On the other hand, the fluorescent dyes **2**, **6** and **9** exhibited a single intense emission band at around 562 nm–599 nm (Φ = 0.62–0.86) and the quantum yields of the isomers **2a**, **6a**, and **9a** exhibited higher Φ values (Φ = 0.86–0.87) than those of the isomers **2b**, **6b**, and **9b** (Φ = 0.62–0.70). Moreover, their fluorescence maxima were red-shifted in the order of **6b** = **9b** < **2b** < **6a** < **9a** < **2a**. The emission wavelength of the **a**-isomer appeared in the long-wavelength side by 26–32 nm than that of the corresponding **b**-isomer. In the comparison of the SS value, it was found that the **a**-isomer exhibited larger SS value of about 4–9 nm than the **b**-isomer, and that the fluorophores including the benzofuran ring exhibited larger SS value of about 30–37 nm than the fluorophores including the benzopyran ring: the order was **6** < **9** < **2**. Though the dipole moments (μ and $\Delta\mu$) of the fluorophores seemed to be deeply related to these differences, we could not find the clear correlation.

Table 2
Spectroscopic properties of the compounds **2, 6** and **9** in 1,4-dioxane.

Compound	Absorption λ_{max}/nm[a] (ε_{max}/dm^3 mol^{-1} cm^{-1})	Fluorescence λ_{max}/nm[b] (Φ[c])	SS[d] $\Delta\lambda_{max}$/nm
2a	541 (36,100), 422 (55,500), 376 (34,000)	599 (0.86)	58
2b	519 (37,800), 395 (60,900), 345 (38,400)	573 (0.71)	54
6a	567 (42,200), 529[e] (22,200), 428 (35,600)	592 (0.86)	25
6b	545 (58,600), 508[e] (27,000), 394 (45,700)	562 (0.62)	17
9a	554 (53,800), 425 (62,300), 404 (39,900)	594 (0.87)	40
9b	531 (54,000), 394 (54,000), 331 (23,680)	562 (0.70)	31

[a] $c = 2.5 \times 10^{-5}$M.
[b] $c = 2.5 \times 10^{-6}$M.
[c] The Φ value was determined with a calibrated integrating sphere system.
[d] Stokes shift value.
[e] Shoulder absorption.

2.5. Spectroscopic properties of symmetric polycyclicphenazine-type fluorescent dyes *2*, *6* and *9* in polymer films

Polylactic acid (PLA), polymethylmethacrylate (PMMA) and polystyrene (PS) were used as polymer medium. The dye-doped polymer films were prepared by casting a polymer solution

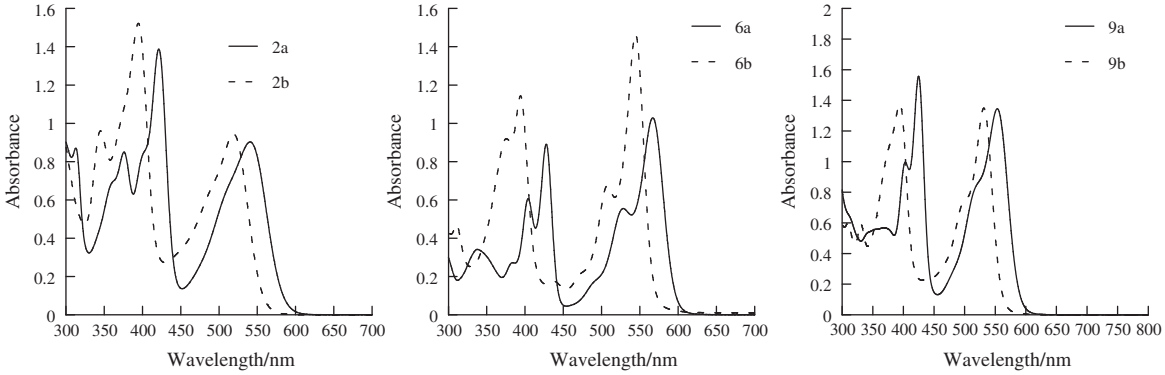

Fig. 3. Absorption spectra of **2a**, **2b**, **6a**, **6b**, **9a** and **9b** in 1,4-dioxane.

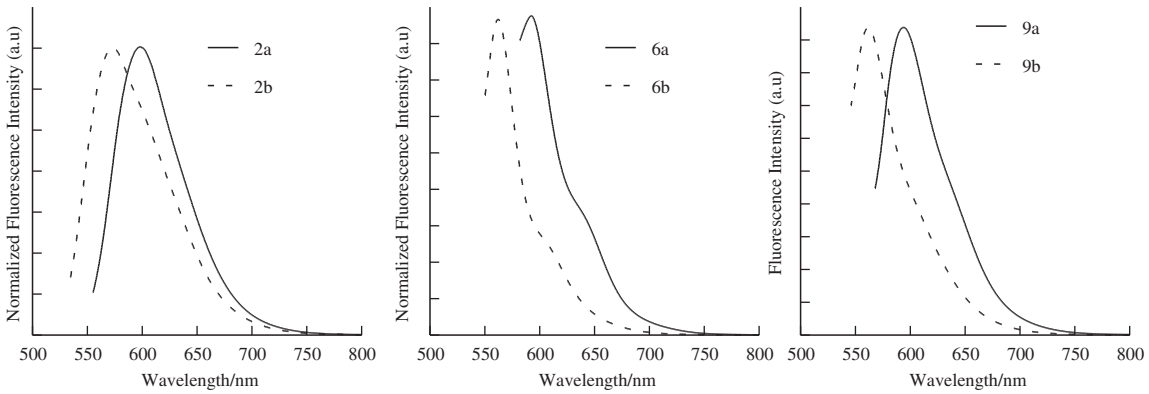

Fig. 4. Fluorescence spectra of **2a**, **2b**, **6a**, **6b**, **9a** and **9b** in 1,4-dioxane.

containing a fluorescent dye on a cover glass. The polymer solution was prepared by dissolving the fluorescent dye and polymer resin pellets in dichloromethane. The concentration of the fluorescent dye was 0.05 wt% and the thickness of the films was ca. 100 μm. The absorption and fluorescence spectra of various fluorescence polymer films were measured. The spectroscopic data are summarized in Table 3 and the absorption and fluorescent spectra of **2a** and **2b** as examples are shown in Figs. 5 and 6, respectively. The isomers **2a** and **2b** showed the absorption band at around 560 nm and 530 nm and the fluorescence band at around 583–613 nm ($\Phi = 0.83$–0.92) and 558–574 nm ($\Phi = 0.63$–0.72), respectively. On the other hand, the isomers **6a** and **6b** showed the absorption band at around 575 nm and 553 nm and the fluorescence band at around 590–600 nm ($\Phi = 0.61$–0.74) and 560–566 nm ($\Phi = 0.17$–0.39), respectively. However, the isomer **6b** was easily decomposed in PLA. In the case of the isomers **9a** and **9b**, only the PS film was

Table 3
Absorption and fluorescence spectral data of the symmetric phenazine-type fluorescent dyes **2**, **6** and **9** in polymer films.

Compound	Medium	Absorption λ_{max}/nm (ε_{max})	Fluorescence λ_{max}/nm (Φ)	SS $\Delta\lambda_{max}$/nm
2a	PLA	561, 427, 379	613 (–)	52
	PMMA	559, 430, 346	602 (0.83)	43
	PS	553, 427, 381	583 (0.92)	30
2b	PLA	530, 399, 351	574 (–)	44
	PMMA	527, 398, 350	573 (0.63)	46
	PS	530, 401, 351	558 (0.72)	28
6a	PLA	575, 432, 409	595 (–)	20
	PMMA	576, 433, 410	602 (0.61)	27
	PS	575, 432, 408	590 (0.74)	15
6b	PLA	–	–	–
	PMMA	(698), 553, 397	566 (0.17)	13
	PS	553, 514, 444	560 (0.39)	7
9a	PS	563, 430, 407	590 (0.82)	27
9b	PS	541, 504, 400	560 (0.61)	19

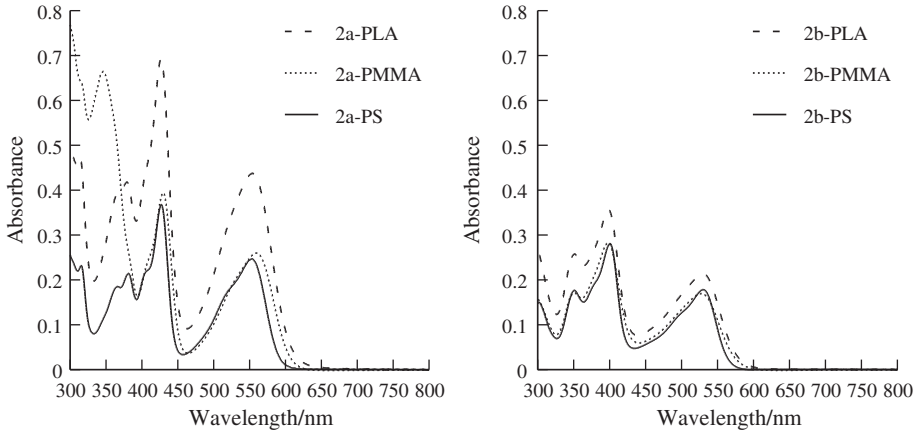

Fig. 5. Absorption spectra of **2a** and **2b** in polymer films.

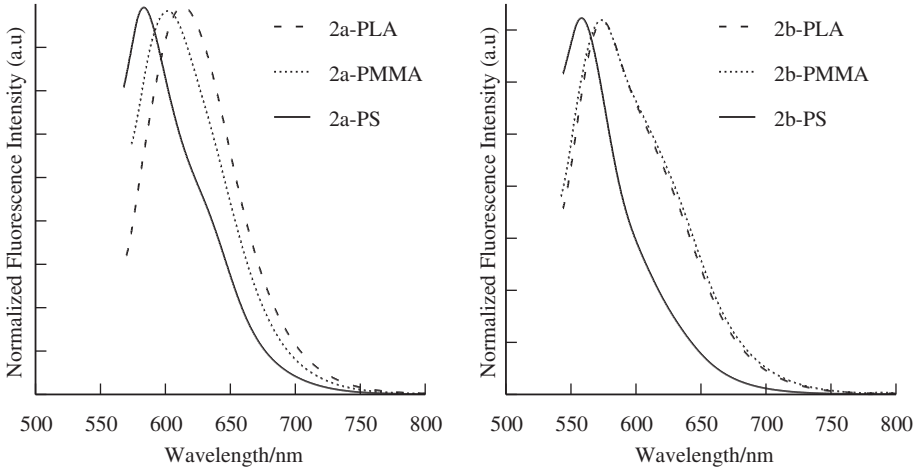

Fig. 6. Fluorescence spectra of **2a** and **2b** in polymer films.

investigated, because the photophysical behaviors of **9** were almost similar to those of **2** and **6**. In the case of the isomers **9a** and **9b**, the dye-doped PS films showed the absorption band at around 563 nm and 541 nm and the fluorescence band at around 590 nm ($\Phi = 0.82$) and 560 nm ($\Phi = 0.61$), respectively. Above data show that the absorption wavelengths are not so affected by the substrate of polymer, but the emission wavelengths are considerably changed. It was suggested that the polarity of polymers influence the stability of the excited state of the fluorescent dyes as similar in solution. Hence, we have investigated the relation between the emission wavelengths of **2** and the dielectric constant of various polymers. The results are summarized in Table 4 and Fig. 7 shows the relation between the emission peak maximum and the dielectric constant of polymer films. It was found that the emission peak tends to be red-shifted with increase in the dielectric constant of polymers. Moreover, the dye-doped PS films exhibited higher quantum yield than the other films, PMMA and PLA.

Table 4
Dielectric constant of polymers and emission peak maxima of mixture of **2a** and **2b**.

Polymer	Dielectric constant (1 MHz) ε'	Emission peak maxima/nm **2**
PS	2.42	586
PLA	2.56	600
EVA	2.60	596
PMMA	2.76	601
PC	2.82	593
APET	2.98	610
PVC	3.59	638

*2.6. Photostabilities of the symmetric polycyclicphenazine-type fluorescent dyes **2**, **6** and **9** in polymer film*

Photostability of the dye-doped polymer films were investigated by use of a xenone accelerated weathering tester (Q-Sun Xe-1). As an example, the absorption and fluorescence spectral changes of the **2a**-doped PS film upon photoirradiation are shown in Fig. 8. The

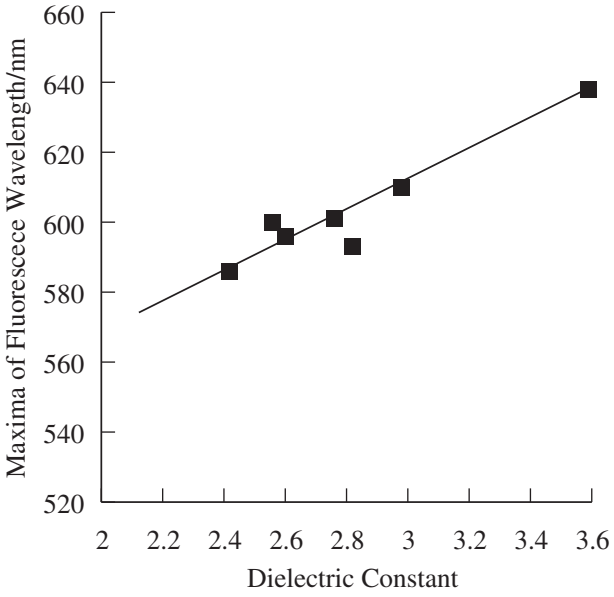

Fig. 7. Plots of the emission peak maxima of mixture of **2a** and **2b** vs dielectric constant of polymers.

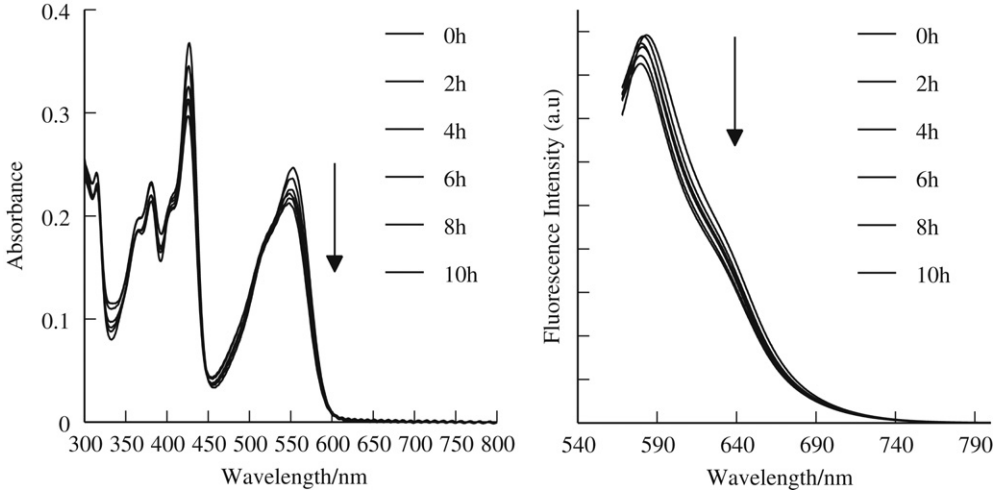

Fig. 8. Absorption and fluorescence spectral changes of the **2a**-doped PS film upon photoirradiation.

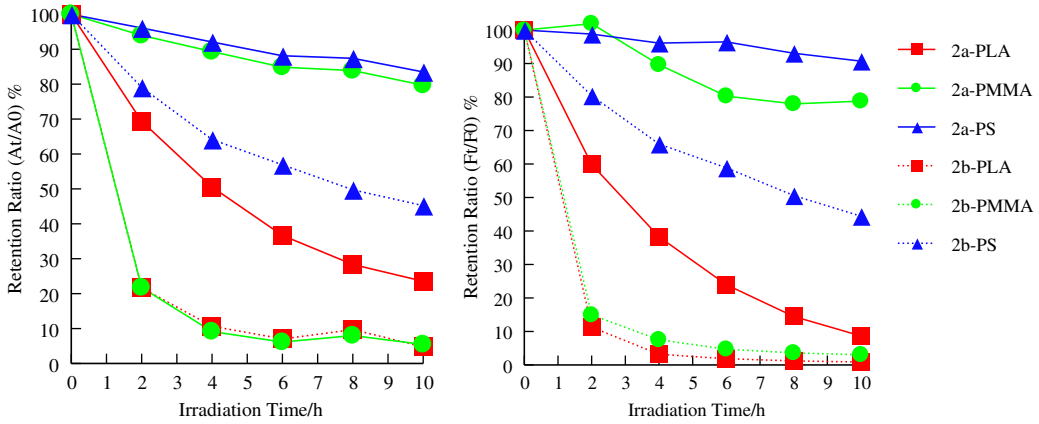

Fig. 9. Plot of the absorption and fluorescence retention ratios vs time in the photofading process of the dye [**2a** and **2b**]-doped polymer films.

maximum absorbance at 561 nm and the maximum fluorescence at 613 nm were gradually decreased. Fig. 9 shows the plot of the absorption and fluorescence retention ratios vs. time in the photofading process of the dyes **2a** and **2b** in polymer films. The retention ratios were calculated by the following equation;

$$\frac{A_t \text{ or } F_t}{A_0 \text{ or } F_0} \times 100 = \text{Retention ratio}(\%)$$

where, A_0, F_0 = Initial maximum absorbance or fluorescence intensity at 0 h, A_t, F_t = Maximum absorbance or fluorescence intensity after t h irradiation.

The data of photostability are summarized in Table 5. It was found that the photofading rate was greatly depend on the polymer substrates; the absorption and fluorescence retention ratios of the dye-doped PS films were higher than those of the dye-doped PMMA and PLA films. Furthermore, the structural **a**-isomers always exhibited higher stability than the **b**-isomers. We have investigated the correlation between the photostability and the dielectric constant of polymers. As shown in Fig. 10, the photostability of dye-doped polymer films seemed to be affected by the dielectric constant. Thus, the dye-doped polymer films of low dielectric constant tend to exhibit higher photostability. Thus, the photostability of the dye-doped polymer films are considerably changed depending on not only the natures of polymer substrate but also the fluorophore's skeleton.

Table 5
Absorption and fluorescence retention ratio of the symmetric phenazine-type fluorescent dyes **2**, **6** and **9** in polymer films.

Compound	Medium	Retention ratio (%) After 10 h	
		Abs.	Flu.
2a	PLA	24	9
	PMMA	80	79
	PS	83	91
2b	PLA	5	1
	PMMA	5	3
	PS	45	44
6a	PLA	21	16
	PMMA	21	28
	PS	84	96
6b	PLA	–	–
	PMMA	0	0
	PS	45	77
9a	PS	79	92
9b	PS	45	64

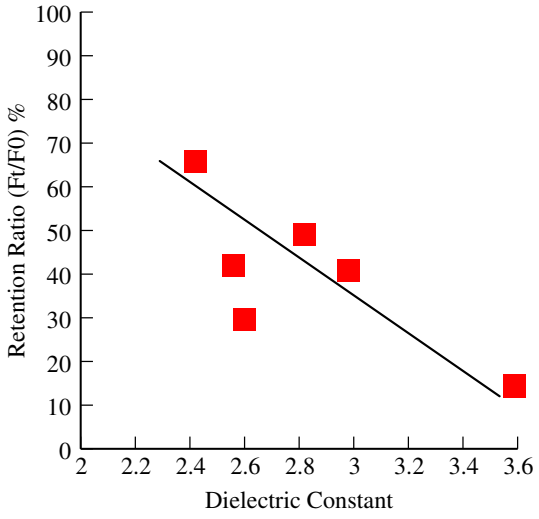

Fig. 10. Plot of emission retention ratio of the compound **2a** vs dielectric constant of polymers.

3. Conclusion

We have designed and synthesized novel polycyclicphenazine-type fluorescent dyes **2a**, **2b**, **6a**, **6b** and **9a**, **9b**, which are structural isomers. These dyes exhibited two strong absorption bands at around 360–430 nm and 520–570 nm and an intense fluorescence band (Φ = 062–0.87) at around 560–600 nm in 1,4-dioxane. The **2a**, **6a**, **9a**-doped PS films showed excellent wavelength conversion function that efficiently convert ultraviolet and green–yellow lights into red light (Φ = 061–0.92) and exhibited good photostability.

4. Experimental

4.1. General

Melting points were determined on Rigaku Thermo Plus 2 system TG8120. IR spectra were recorded on a JASCO FT/IR-5300 spectrometer for sample in KBr pellet form. Absorption spectra were observed with a JASCO UV-670 spectrophotometer and fluorescence spectra were measured with a JASCO FP-6600 spectrophotometer. The fluorescence quantum yields (Φ) of solutions and the crystals were determined by a Hamamatsu C9920-12, which

have absolute quantum yield measurement systems, by using a calibrated integrating sphere. Elemental analyses were recorded on a Perkin Elmer 2400 II CHN analyzer. ^{1}H-NMR spectra were recorded on a JNM-LA-400 (400 MHz) FT NMR spectrometer with tetramethylsilane (TMS) as an internal standard. Column chromatography was performed on silica gel (KANTO CHEMICAL, 60N, spherical, neutral).

4.2. Synthesis of compounds **2a** and **2b**

A solution of *o*-quinone **1** (5.00 g, 13.2 mmol) and ammonium acetate (16.42 g, 21.3 mmol) in acetic acid was stirred at 100 °C for 3 h. The reaction mixture was poured into cold water and then the causing precipitate was filtered. The resulting residue was dissolved with CH_2Cl_2 and washed with water. The organic layer was evaporated and the residue was chromatographed on silica gel (xylene as eluent) to give **2a** (0.84 g, yield 18%) as red powder and **2b** (0.96 g, yield 20%) as orange power, respectively.

Compound **2a**: d.p. 313 °C; IR(KBr)/cm^{-1}: 2955, 2927, 2869, 2361, 1626, 1524, 1502; ^{1}H-NMR ($CDCl_3$,TMS) δ = 1.04 (t, J = 7.56 Hz, 12H), 1.46 (tq, J = 7.56, 7.32 Hz, 8H), 1.72 (tt, J = 7.80, 7.32 Hz, 8H), 3.44 (t, J = 7.80 Hz, 8H), 6.89 (dd, J = 8.76, 2.20 Hz, 2H), 7.13 (d, J = 1.96 Hz, 2H), 7.83 (dd, J = 8.04 Hz, 2H), 7.92 (dd, J = 8.04 Hz, 2H), 8.19 (d, J = 8.76 Hz, 2H), 8.61 (d, J = 7.56 Hz, 2H), 9.74 (d, J = 8.04 Hz, 2H); elemental analysis calcd (%) for $C_{48}H_{50}N_4O_2$: C 80.64, H 7.05, N 7.84; found: C 80.55, H 7.11, N 7.93.

Compound **2b**: d.p. 277 °C; IR(KBr)/cm^{-1}: 2953, 2928, 2869, 1627, 1512; ^{1}H-NMR ($CDCl_3$,TMS) δ = 1.05 (t, J = 7.20 Hz, 12H), 1.46 (qt, J = 7.20 Hz, 8H), 1.70 (tt, J = 7.20 Hz, 8H), 3.41 (t, J = 7.20 Hz, 8H), 6.84 (dd, J = 8.80, 2.00 Hz, 2H), 7.08 (d, J = 2.00 Hz, 2H), 7.75–7.85 (m, 4H), 8.13 (d, J = 9.20 Hz, 2H), 8.52 (d, J = 7.20 Hz, 2H), 9.62 (dd, J = 8.00, 1.20, 2H); elemental analysis calcd (%) for $C_{48}H_{50}N_4O_2$: C 80.64, H 7.05, N 7.84; found; C 80.35, H 7.23, N 7.86.

4.3. Synthesis of compound **4**

A solution of *o*-quinone **3** (0.50 g, 1.33 mmol) and hydroxylamine hydrochloride (6.66 g, 95.9 mmol) in pyridine was stirred under reflux for 3 h. The reaction mixture was poured into cold water. The precipitate was filtered and the residue was washed with diluted hydrochloric acid and water. The residue was chromatographed on silica gel (CH_2Cl_2:ethyl acetate = 20:1 as eluent).

4.4. Synthesis of compound **5**

A solution of **4** (0.40 g, 0.98 mmol), tin(II) chloride (1.86 g, 9.81 mmol) and hydrochloric acid (5 ml) in ethanol was stirred at 78 °C for 2 h. After the reaction, the reaction mixture was poured into water and the precipitate was filtered. Further purification was not performed because the product was unstable in air.

4.5. Synthesis of compounds **6a** and **6b**

A solution of *o*-quinone **1** (0.37 g, 0.98 mmol) and the compound **5** in ethanol was stirred at reflux for 10 h. After the reaction, the solvent was evaporated and the residue was extracted with CH_2Cl_2 and washed with water. The combined organic layer was evaporated. The resulting residue was chromatographed on silica (CH_2Cl_2 as eluent) to give **6a** (0.32 g, 46% yield) as red powder and **6b** (0.04 g, 5% yield) as orange powder, respectively.

Compound **6a**: d.p.306 °C; IR(KBr)/cm^{-1}: 2955, 2929, 2869, 2360, 2342, 1600, 1523; ^{1}H-NMR ($CDCl_3$) δ = 1.01 (t, J = 7.56 Hz, 12H), 1.42 (qt, J = 7.56 Hz, 8H), 1.62–1.69 (m, 8H), 3.36 (t, J = 7.56 Hz, 8H), 6.39 (d, J = 2.68 Hz, 2H), 6.59 (dd, J = 9.04, 2.44 Hz, 2H), 7.34 (d, J = 7.08 Hz, 2H), 7.70 (dd, J = 8.04 Hz, 2H) 7.89 (s, 2H), 7.92 (d, J = 9.04 Hz, 2H), 8.91 (d, J = 8.04 Hz, 2H); elemental analysis calcd (%) for $C_{48}H_{50}N_4O_2$: C 80.64, H 7.05, N 7.84; found; C 80.30, H 7.12, N 7.89.

Compound **6b**: d.p.321 °C; IR(KBr)/cm^{-1}: 2936, 2859, 2360, 2342, 1596, 1523; ^{1}H-NMR ($CDCl_3$) δ = 1.01 (t, J = 7.32 Hz, 12H), 1.42 (qt, J = 7.32 Hz, 8H), 1.62–1.70 (m, 8H), 3.36 (t, J = 7.32 Hz, 8H), 6.37 (d, J = 2.20 Hz, 2H), 6.58 (dd, J = 8.80, 2.20 Hz, 2H), 7.30 (d, J = 7.60 Hz, 2H), 7.70 (dd, J = 7.56 Hz, 2H) 7.76 (s, 2H), 7.87 (d, J = 9.00 Hz, 2H), 8.99 (d, J = 7.84 Hz, 2H); elemental analysis calcd (%) for $C_{48}H_{50}N_4O_2$: C, 80.64; H, 7.05; N, 7.84; found; C, 80.26; H, 7.25; N, 7.91.

4.6. Synthesis of compound **7**

A solution of *o*-quinone **1** (2.00 g, 5.33 mmol) and hydroxylamine hydrochloride (26.65 g, 384 mmol) in pyridine was stirred at reflux for 7 h. After the reaction, the reaction mixture was poured into water. The resulting precipitate was washed with diluted hydrochloric acid and water. The residue was chromatographed on silica (CH_2Cl_2 as eluent).

4.7. Synthesis of compound **8**

A solution of **7** (0.44 g, 1.08 mmol), tin(II) chloride (2.05 g, 10.08 mmol) and hydrochloric acid (5 ml) in ethanol was stirred at 78 °C for 4 h. After the reaction, the reaction mixture was poured into water and the precipitate was filtered. Further purification was not performed because the product was unstable in air.

4.8. Synthesis of compounds **9a** and **9b**

A solution of *o*-quinone **3** (0.41 g, 1.08 mmol) and the compound **8** (0.41 g, 1.08 mmol) in ethanol was stirred at reflux for 10 h. After the reaction, the solvent was evaporated and the resulting residue was dissolved with CH_2Cl_2 and washed with water. The combined organic layer was evaporated and the residue was chromatographed on silica (xylene as eluent) to give **9a** (0.29 g, 38% yield) as red powder and **9b** (trace) as orange powder.

Compound **9a**: d.p.255 °C; IR (KBr)/cm^{-1}: 2955, 2930, 2870, 2359, 2342, 1627, 1600; ^{1}H-NMR ($CDCl_3$) δ = 1.02 (t, J = 7.32 Hz, 6H), 1.03 (t, J = 7.32 Hz, 6H), 1.38–1.50 (m, 8H), 1.60–1.75 (m, 8H), 3.35 (t, J = 7.32 Hz, 4H), 3.43 (t, J = 7.56 Hz, 4H), 6.37 (d, J = 1.95 Hz, 1H), 6.58 (dd, J = 8.56, 2.32 Hz, 1H), 6.86 (dd, J = 8.78, 1.95 Hz, 1H), 7.10 (d, J = 1.72 Hz, 1H) 7.36 (d, J = 7.81 Hz, 1H), 7.71–7.78 (m, 2H), 7.87 (dd, 8.08 Hz, 1H), 7.92 (dd, J = 4.64 Hz, 2H), 8.15 (d, J = 8.78 Hz, 1H), 8.52 (d, J = 7.81 Hz, 1H), 9.12 (d, J = 8.05 Hz, 1H), 9.48 (d, J = 8.05 Hz, 1H); elemental analysis calcd (%) for $C_{48}H_{50}N_4O_2$: C 80.64, H 7.05, N 7.84; found; C 80.39, H 6.96, N 7.67.

Compound **9b**: d.p.202 °C; IR(KBr)/cm^{-1}: 2955, 2932, 2858, 2360, 2342, 1630, 1600, 1522; ^{1}H-NMR ($CDCl_3$) δ = 1.00–1.05 (m, 12H), 1.38–1.49 (m, 8H), 1.58–1.74 (m, 8H), 3.34 (t, J = 7.56 Hz, 8H), 3.41 (t, J = 7.56 Hz, 2H), 6.34 (d, J = 2.16 Hz, 2H), 6.58 (dd, J = 9.04, 2.20 Hz, 1H), 6.85 (dd, J = 8.80 Hz, 1H), 7.08 (d, J = 1.96 Hz, 1H), 7.31 (d, J = 7.80 Hz, 1H), 7.69–7.85 (m, 4H), 8.01 (s, 1H), 8.13 (d, J = 8.80 Hz, 1H), 8.51 (d, J = 7.80 Hz, 1H), 9.05 (d, J = 8.04 Hz, 1H), 9.54 (d, J = 8.08 Hz, 1H); elemental analysis calcd (%) for $C_{48}H_{50}N_4O_2$: C 80.64, H 7.05, N 7.84; found; C 80.62, H 7.38, N 7.80.

4.9. Computational methods

All calculations were performed on a FUJITSU FMV-ME4/657. The semi-empirical calculations were carried out with the WinMOPAC Ver. 3 package (Fujitsu, Chiba, Japan). Geometry calculations in the ground state were carried out using the PM3 method. All geometries were completely optimized (keyword PRECISE) by the eigenvector following routine (keyword EF). Experimental

absorption spectra of the symmetric phenazine derivatives were studied with the semi-empirical method INDO/S (intermediate neglect of differential overlap/spectroscopic). All INDO/S calculations were performed using single excitation full SCF/CI (self-consistent field/configuration interaction), which includes the configurations with one electron excited from any occupied orbital to any unoccupied orbital, 225 configurations were considered for the configuration interaction [keyword CI (15 15)].

4.10. X-ray crystal structure determinations

The reflection data were collected at 23 ± 1 °C on a Rigaku AFC7S four-circle diffractometer by $2\theta-\omega$ scan technique, and using graphite-monochromated Mo-Kα ($\lambda = 0.71069$ Å) radiation at 50 kV and 40 mA. The data were corrected for Lorentz and polarization effects. All calculations were performed using the CrystalStructure [22,23] crystallographic software package. CCDC-827536 (**2b**) contains the supplementary crystallographic data for this paper. These data can be obtained free of charge from the Cambridge Crystallographic Data Centre via www.ccdc.cam.au.uk/data_request/cif.

Compound **2b**: Crystal of **2b** was recrystallized from CH_2Cl_2 as red plate, air stable. The one selected had approximate dimensions 0.80 × 0.60 × 0.10 mm. The transmission factors ranged from 0.882 to 0.980. The crystal structure was solved by direct methods using SIR2004 [24]. The structures were expanded using Fourier techniques [25]. The non-hydrogen atoms were refined anisotropically. Some hydrogen atoms were refined isotropically, the rests were fixed geometrically and not refined.

Crystal data. $C_{48}H_{50}N_4O_2 \cdot CH_2Cl_2$, $M = 799.88$, monoclinic, $a = 17.133(4)$, $b = 27.221(7)$, $c = 9.277(5)$ Å, $\beta = 100.89(3)^\circ$, $V = 4248.4(25)$ Å^3, space group $P2_1/a$ (#14), $Z = 4$, 8093 reflections measured, 7948 unique ($R_{int} = 0.697$) which were used in all calculations. The final R indices were $R_1 = 0.0765$, $wR(F^2) = 0.3578$ (all data).

Acknowledgments

This work was partially supported by a Grant-in-Aid for Science and Research from the Ministry of Education, Science, Sport and Culture of Japan (Grant 21550181) and by a Adaptable and Seamless Technology Transfer Program through Target-driven R&D of Japan Science and Technology Agency (JST).

References

[1] Rajapakse NC, Kelly JW. Regulation of chrysanthemum growth by spectral filters. J Amer Soc Hort Sci 1992;117:481–5.
[2] Noè N, Eccher T, Signore ED, Montoldi A. Growth and proliferation *in vitro* of *Vaccinium corymbosum* under different irradiance and radiation spectral composition. Biol Plant 1998;41:161–7.
[3] Oyaert E, Volckaert E, Debergh PC. Growth of chrysanthemum under coloured plastic films with different light qualities and quantities. Sci Hort 1999;79:195–205.
[4] Muleo R, Molini S. Light quality regulated shoot cluster growth and development of MM106 apple genotype in *in vitro* culture. Sci Hort 2006;108:364–70.
[5] Oberhaus L, Briand JF, Leboulanger C, Jacquet S, Humbert JF. Comparative effects of the quality and quantity of light and temperature on the growth of *Planktothrix agardhi* and *P. rubescens*. J Phycol 2007;43:1191–9.
[6] Molini S, Muleo R. Effect of light quality on micropropagation of woody species. In: Jain, Ishii, editors. Micropropagation of woody trees and fruits. Dordrecht, The Netherlands: Kluwer Academic Publishers; 2003. p. 3–35.
[7] D'Onofrio C, Molini S. Effects of light quality on induction and growth of MM106 apple callus cultures. Adv Hort Sci 2004;16:47–52.
[8] Hamada K, Shimasaki K, Nishimura Y, Egawa H, Yoshida K. Effect of red fluorescent films on proliferation of *Cymbidium finlaysonianum* Lindl. PLB cultured *in vitro*. Hort. Env. and Biotechnol 2009;50:319–23.
[9] Hemming S, van Os EA, Hemming J, Dieleman JA. The effect of new developed fluorescent greenhouse films on the growth of *fragaria x ananassa* 'Elsanta'. Eur J Hort Sci 2006;71:145.
[10] Kittas C, Baille A. Determination of the spectral properties of several greenhouse cover materials and evaluation of specific parameters related to plant response. J Agric Eng Res 1998;71:193.
[11] Hamada K, Shimasaki K, Ogata T, Nishimura Y, Nakamura K, Ooyama EH, et al. Effects of spectral composition conversion film and plant growth regulators on proliferation of *Cymbidium protocorm* like body (PLB) cultured *in vitro*. Environ Control Biol 2010;48:127–32.
[12] Yoshida K, Shimasaki K, Egawa H, Hamada K. JP Patent Publication 2010;884–920.
[13] Stewart JJP. Optimization of parameters for semiempirical methods I. Method. J Comput Chem 1989;10:209.
[14] Ridley JE, Zerner MC. An intermediate neglect of differential overlap technique for spectroscopy: pyrrole and the azines. Theor Chim Acta 1973;32:111.
[15] Ridley JE, Zerner MC. Triplet states via intermediate neglect of differential overlap: benzene, pyridine and the diazines. Theor Chim Acta 1976;42:223.
[16] Bacon AD, Zerner MC. An intermediate neglect of differential overlap theory for transition metal complexes: Fe, Co and Cu chlorides. Theor Chim Acta 1979;53:21.
[17] Adachi M, Murata Y, Nakamura S. The relationship between the structures and absorption spectra of cyan color indoaniline dyes. J Org Chem 1993;58:5238–44.
[18] Fabian WMF, Schuppler S, Wolfbesis OS. Effects of annulation on absorption and fluorescence characteristics of fluorescein derivatives: a computational study. J Chem Soc Perkin Trans 1996;2:853–6.
[19] Ooyama Y, Okamoto T, Yamaguchi T, Suzuki T, Hayashi A, Yoshida K. Heterocyclic quinol-type fluorophores: synthesis, X-ray crystal structures, and solid-state photophysical properties of Novel 5-hydroxy-5-substituentbenzo[b]naphtho [1,2-d]furan-6-one and 3-hydroxy-3-substituentbenzo[kl]xanthen-2-one derivatives. Chem Eur J 2006;12:7827.
[20] Katritzky AR. Handbook of heterocyclic chemistry. Oxford: Pergamon Press; 1985. p. 432.
[21] Katritzky AR. Comprehensive heterocyclic chemistry. Chairman Ed., vol. 3. Oxford: Pergramon Press; 1984. p. 179.
[22] Crystal Structure 3.8: Crystal structure analysis package, Rigaku and Rigaku/MSC (2000–2006). 9009 New Trails Dr. The Woodlands TX 77381 USA.
[23] Carruthers JR, Rollett JS, Betteridge PW, Kinna D, Pearce L, Larsen A. Chemical Crystallography Laboratory, Oxford, UK; 1999.
[24] Burla MC, Caliandor R, Camalli M, Carrozzini B, Cascarano GL, De Caro L, et al. *SIR2004*: an improved tool for crystal structure determination and refinement. J Appl Cryst 2005;38:381.
[25] DIRDIF99 Beurskens PT, Admiraal G, Beurskens G, Bosman WP, de Gelder R, Israel R, et al. The DIRIF99 program system. Technical report of the crystallography laboratory. The Netherlands: University of Nijmegen; 1999.